Int. J. Therm. Sci. (2000) 39, 1056–1065

S1290-0729(00)01194-7/FLA

Local measurements in the flow of a steam injector and visualisation

Nicolas Deberne [a], Jean-François Leone [b]*, André Lallemand [b]

[a] *EDF/SEPTEN, 12-14 Av. Dutriévoz, 69628 Villeurbanne cedex, France*

[b] *CETHIL, UMR 5008, INSA de LYON, 20 Av. Albert Einstein, 69621 Villeurbanne cedex, France*

(Received 7 June 2000, accepted 7 September 2000)

Abstract — A steam injector is a thermocompression device where the steam drags directly a subcooled liquid and delivers a liquid with an outlet pressure higher than both upstream fluid pressures. The functioning principle of injectors involves sophisticated thermohydraulic processes whose present knowledge is essentially empirical. This work presents an experimental approach of steam injector in order to finely understand and quantify the physical laws driving the flow in the mixing chamber. Local measurements (2D) are carried out on a special device with a rectangular section, where the flow was visualised. These measurements are the void fraction, the static pressure and the static temperature. They permit the calculation of all the variables and a well understanding of the physical phenomena involved in the flow. Especially, we show, in some well-defined zones, the existence of important non-equilibrium kinetic, thermal and thermodynamic phenomena. © 2000 Éditions scientifiques et médicales Elsevier SAS

heat transfer / mass transfer / condensation / injector / visualisation

Nomenclature

A	interface density area	$m^2 \cdot m^{-3}$
C_p	specific heat	$J \cdot kg^{-1} \cdot K^{-1}$
H	heat transfer coefficient	$W \cdot m^{-2} \cdot K^{-1}$
H_t	total enthalpy flow rate	W
h	specific enthalpy	$J \cdot kg^{-1}$
k	slip ratio $= u_V/u_L$	
M	mass flow rate	$kg \cdot s^{-1}$
L	latent heat of vaporisation	$J \cdot kg^{-1}$
L_m	mixing chamber length	m
P	static pressure	Pa
Q	density of heat flux	$W \cdot m^{-3}$
s	entropy	$J \cdot kg^{-1} \cdot K^{-1}$
S	section area	m^2
T	static temperature	K
u	velocity	$m \cdot s^{-1}$
U	mass flow rate ratio $= M_L/M_V$	
x	abcissa of the mixing chamber	m
x_v	quality in the mixing chamber	
$x_{v,v}$	quality in the "vapour" flow	

Greek symbols

α	void fraction	
Γ	condensation mass flux	$kg \cdot m^{-3} \cdot s^{-1}$
ρ	density	$kg \cdot m^{-3}$

Subscripts

i	with reference to abciss
L	liquid
m	mixing
V	vapour
0	inlet
3	outlet

1. INTRODUCTION

A steam injector is a simple, compact and passive device in which steam is used as the energy source to pump cold water at a pressure lower than the steam and to produce an outlet liquid, which is at a pressure higher than the steam inlet pressure. Its main characteristic is that no moving parts are needed for its functioning, thermodynamic processes relying on direct transfers of mass momentum and heat between the two phases.

* Correspondence and reprints.
jfl@genserver.insa-lyon.fr

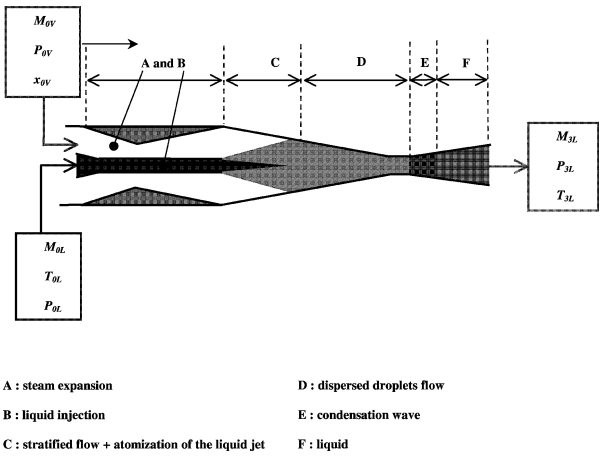

Figure 1. Schematic representation of the steam injector.

The steam injector can be used as a safety pump in a light water reactor, while a steam supply is generally available in power plants. In this case a high-pressure water supply can be useful for heat removal in case of accident. Moreover, it is a passive system without rotating machinery and its functioning requires no external energy supply.

Figure 1 shows a steam injector schematic, divided in five regions. In the first part called the steam nozzle (A), which has a converging–diverging shape, the steam is accelerated to a supersonic velocity owing to a nearly isentropic expansion. The water nozzle or the liquid injector (B) distributes water. Here, the chosen arrangement is a central water nozzle and an annular outer steam nozzle. It will be seen in the following that functioning depend on the arrangement [1]. This arrangement can be easily taken into account in the model. In the mixing region (C, D), steam and water exchange heat, momentum (due to temperature and velocity differences) and mass (due to condensation of steam on water droplets extracted from the water cone at the exit of the water nozzle). Condensation is achieved in the shock wave occurring at the exit of the mixing section (E). The major pressure rise is realised in this shock wave. Then, water is decelerated in the diffuser (F) and kinetic energy is furtherly converted into a pressure increase.

Although the technology of the steam injector has been known for about one century, its modelling still represents a not completely solved problem. Experiments have been made by Rose [2], Grolmes [3] and Alad'yev et al. [4, 5] in past years. More recently, its possible use for nuclear power plants has involved new studies: Manno and Dehbi [6], Narabayashi et al. [7], Chisacof and Lallemand [8], Léone et al. [9] and Cattadori et al. [10].

A numerical modelling able to accurately predict the steam injector performance does not exist. Two major problems explain these difficulties: on the one hand the physical phenomena which occur in the mixing chamber (two-phase flow with simultaneous exchange of mass, momentum and energy), on the other hand, the difficulty of a numerical treatment taking into account the global map of two-phase flow (void fraction range from one to zero). A complete and accurate modelling of steam injector represents a big challenge for the next years.

This experimental work permits a physical valuation of the flow occurring in the mixing chamber. In order to quantify and analyse the physical laws governing the flow, we realised local measurements. As a first step, these laws can be inserted in numerical codes.

2. LOCAL MEASUREMENTS IN THE MIXING CHAMBER OF A STEAM INJECTOR

The principal aim of this work is to experimentally determine the thermohydraulic variables in the mixing chamber of the steam injector. Considering that the flow is approximately one-dimensional, these variables are:

– α the void fraction,

– u_V and u_L the vapour and liquid velocities,

– P_V and P_L the static pressures,

– T_V and T_L the static temperatures,

– $x_{v,v}$ is the quality of the "vapour" flow at the entrance of the mixing chamber.

The measurements of the thermohydraulic variables require that the flow is adiabatic and in steady state conditions. The flow is governed by two invariants: the total enthalpy flow rate H_t and the mass flow rate M, which reduce the number of independent variables to five.

2.1. Experimental apparatus and visualisation of the flow in the mixing chamber

In order to better understand the geometry of the flow and to optimise the sensor locations, a special device was designed for these experiments (*figure 2*).

This device is a converging–diverging nozzle with a rectangular section, 8 mm in thickness. It was designed

according to respect the main similarity ratio of the geometrical parameters used for other injectors (axisymmetric) previously tested in the laboratory [11]. This thickness was designed and optimised for a good transmission of white light in the flow without 3D effect induced by the viscous limit layer developed at the wall. The steam injector is in horizontal position.

The visualisation of the flow in the mixing chamber is realised with an analogic camera and a source of white light of 1 000 W. Some experimentations are carried out with a high speed camera (8 000 pictures·s^{-1}) specially to visualise the flow at the start of the process and the break up of the liquid jet. Two configurations were used for this experiment:

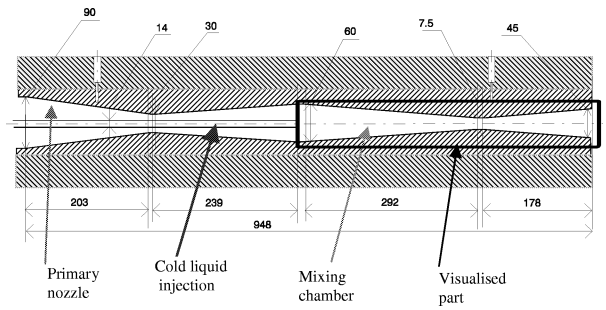

Figure 2. Steam injector device for visualisation and measurements (longitudinal view) length in mm.

– a back lighting of the flow, where the camera is located in the opposite side of the light source (*figure 3(a)*). This configuration permits to visualise the dispersed zone of the flow (specially droplets in the vapour phase);

– a front lighting of the flow, where the camera is located in the same side of the light source (*figure 3(b)*). This configuration is better for showing the density variation in the flow.

The test bench operates in a closed loop where it is possible to independently vary steam pressure, liquid temperature, liquid pressure and back-pressure. The steam and water flow rates were measured by means of calibrated orifice plate and multiple Pitot tube (Annubar), respectively. Temperatures and pressures were measured by K-type thermocouples and by resistive pressure transducers, respectively. The range of the independent parameters explored in the test program is given in *table I*. No modifications of the structure of the flow were noted during these tests. The evolutions of the parameters measured inside the mixing section are similar for all conditions given in *table I*. Therefore, we present here only the results for the conditions given in *table II*. These condi-

TABLE I
Range of independent variables

P_{0V} (bar)	$X_{0V,V}$	P_{0L} (bar)	T_{0L} (°C)	P_{3L} (bar)
4–8	0.95–1	1.1–3.2	15–40	2–5

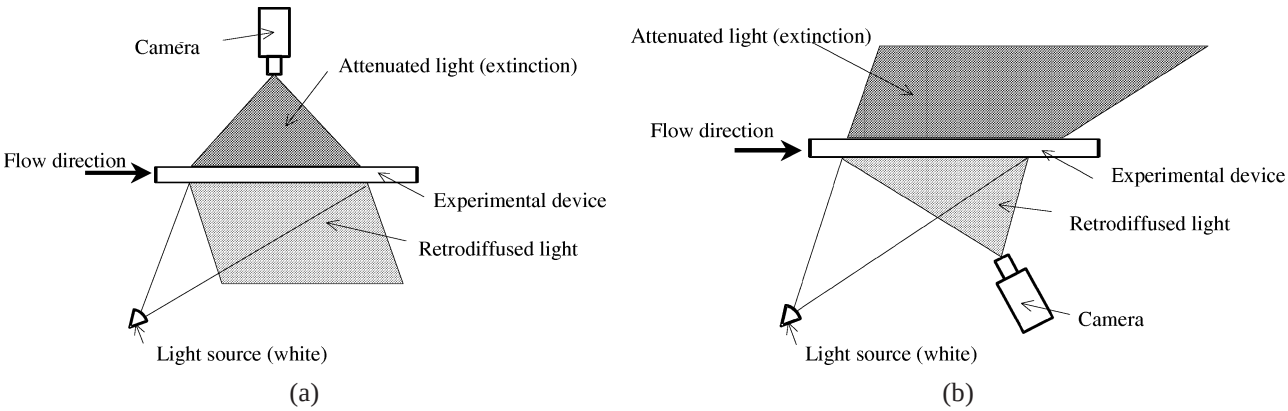

Figure 3. (a) Configuration with back lighting. (b) Configuration with front lighting.

TABLE II
Experimental conditions for measurements

M_{0V} (kg·s^{-1})	P_{0V} (bar)	T_{0V} (°C)	M_{0L} (kg·s^{-1})	P_{0L} (bar)	T_{0L} (°C)	M_{3L} (kg·s^{-1})	P_{3L} (bar)	T_{3L} (°C)	U
0.1	6.06	157.9	1.056	2.1	15.2	1.155	3.6	70.0	10.58

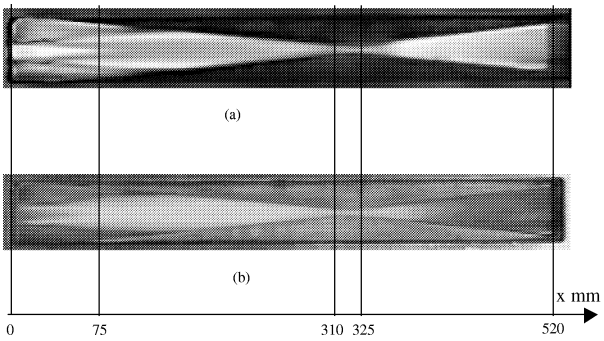

Figure 4. (a) Visualisation of the flow in the mixing chamber with back lighting. (b) Visualisation of the flow in the mixing chamber with front lighting.

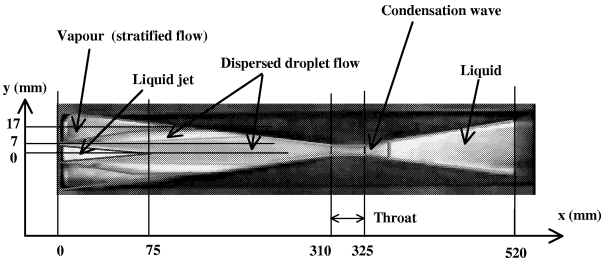

Figure 5. Mesh for the measurements.

tions remain the same for all experiments in order to have a same reference point for all measurements.

Figures 4(a) and *4(b)* show a stratified flow composed of a central liquid jet surrounded by the vapour phase (zone 0 mm $< x <$ 75 mm, *figure 5*). After this zone, a fine dispersed droplet zone appears resulting from atomisation of the jet liquid. After the throat, *figure 4(a)* shows a clear zone in the diffuser (365 mm $< x <$ 520 mm), showing that the flow is single phase (liquid).

The flow visualised in the mixing chamber allows to define three pertinent lines useful for the measurement mesh (*figure 5*):

– one line located in the vapour part of the stratified flow ($y = 17$ mm),

– one line located just at the base of the liquid jet ($y =$ 7 mm),

– one line located in the center of the liquid jet ($y =$ 0 mm).

2.2. Void fraction measurement

The void fraction measurement is realised with the gamma-ray attenuation method. For our experiments,

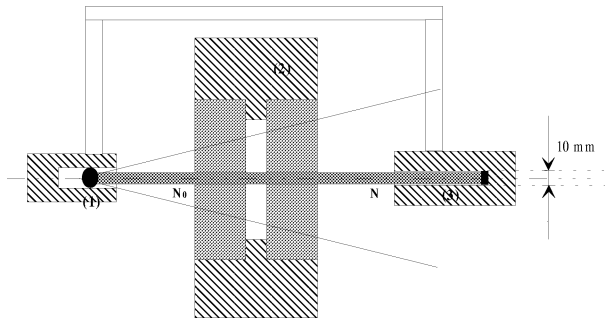

Figure 6. Experimental apparatus for the void fraction measurements: (1) source, (2) device, (3) detector, N_0 = number of emitted photons by the source, N = number of received photons by the detector.

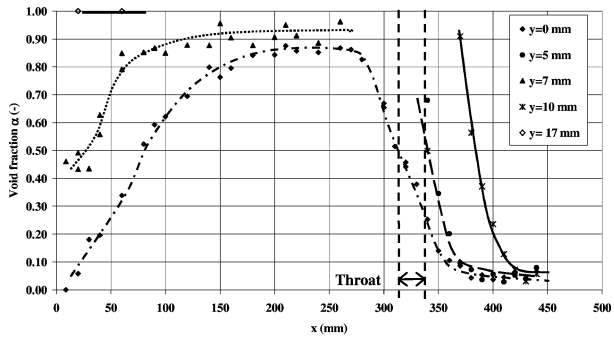

Figure 7. Void fraction profiles in mixing chamber.

this method is the most accurate for a two-phase flow with a large range of void fractions (near one to zero). The experimental apparatus (*figure 6*) is composed of a radioactive source (americium), a collimator and a photon detector. Each photon emitted from the source crosses the thickness of the flow and is absorbed or not by the water. Using a high-energy ray like gamma-ray, the attenuation of the incident flux is only due to absorption phenomena (diffraction or diffusion does not contribute to the global attenuation flux). The counting rate (ratio of received photons to incident photons) depending on the flow density can be easily correlated with the void fraction. Uncertainty of the measurements, taking into account sensor accuracy, is equal to $\Delta\alpha = 0.05$ for a counting time of 20 s.

The void fraction profiles are shown in *figure 7* for the operating conditions given in *table II*. *Figure 7* shows an increase of void fraction in the center line ($y = 0$) due to:

– the atomisation of the liquid jet,

– the reduction of the slip ratio between the vapour and the liquid.

The void fraction can be related to the slip ratio, the steam quality and the densities by the following expression:

$$\alpha = \frac{x_V \rho_L}{k\rho_V(1-\rho_V)+\rho_l x_V} \quad (1)$$

The effects of the steam quality on the void fraction are illustrated in *figure 8* where the void fraction is plotted against the slip ratio. A plot of void fraction versus steam quality is shown in *figure 9*.

As shown in *figure 8*, the void fraction is mainly sensitive to the slip ratio for the range of steam quality ($0.001 < x_V < 0.1$), with an increase of void fraction when the slip ratio decreases. In the first zone ($0\ \text{mm} < x < 150\ \text{mm}$ and $x_V \approx 0.1$), the vapour is decelerated by the droplets generated by the liquid jet atomisation. This phenomenon reduces progressively the slip ratio and explains the increase of mean void fraction at the entrance of the mixing chamber. After this zone, the void fraction becomes nearly constant ($\alpha = 0.9$) and shows that the flow is fully dispersed. The mean diameter of the droplets, calculated with atomisation correlation of Monote [12], is 5 μm.

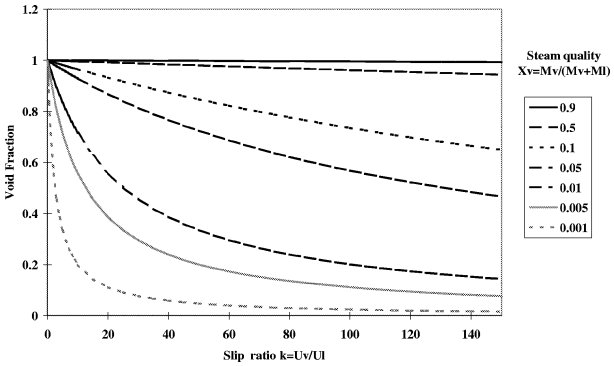

Figure 8. Void fraction dependence with the reduction of the slip ratio ($\rho_L = 1\,000\ \text{kg·m}^{-3}$ and $\rho_V = 0.4\ \text{kg·m}^{-3}$).

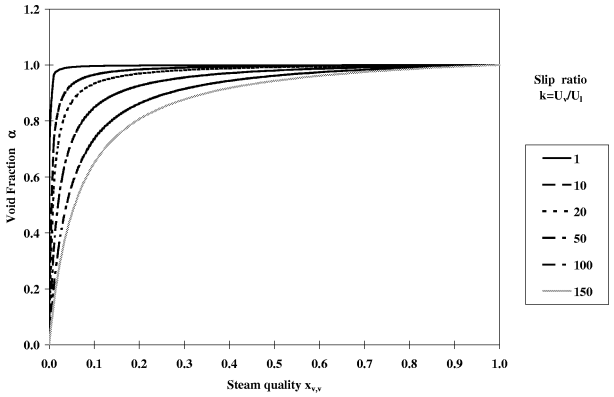

Figure 9. Void fraction dependence with the flow quality ($\rho_L = 1\,000\ \text{kg·m}^{-3}$ and $\rho_V = 0.4\ \text{kg·m}^{-3}$).

Behind the throat, *figure 7* shows a high decrease of void fraction, which is characteristic of the condensation wave (extinction of the vapour phase). As shown in *figure 9*, the void fraction varies greatly with the steam quality ($0.0 < x_V < 0.01$ and the slip ratio $k \approx 1$). That explains the fast decrease of the void fraction in the condensation wave zone.

2.3. Static pressure measurement

The measurement of static pressure is realised with relative sensors (range [0; 8 bar]) and differential sensors (range [−0.4; +0.4 bar]). Uncertainty of the measurements, taking into account sensors accuracy, experimental fluctuations and statistical treatment, is lower than 1.5 %. For the operating conditions given in *table II*, *figure 10* shows that the static pressure fields for the vapour ($y = 17$ mm) and for the liquid ($y = 0$ mm) are decoupled at the entrance of the mixing chamber. At the interface of the jet the liquid pressure is equal to the liquid-vapour equilibrium pressure. The vapour continues to expand until it encounters the liquid jet or droplets due to atomisation. When the vapour encounters the liquid phase, it is suddenly decelerated and it transmits its impulsion to the liquid phase. These phenomena explain the small increase of the liquid pressure, which is observed in the zone $25 < x < 75$ mm.

Downstream the liquid jet, the static pressure becomes constant (the mixing flow is also in quasi-equilibrium). In the part where the flow is homogeneous, the pressure is altered by the high condensation rate, involving a

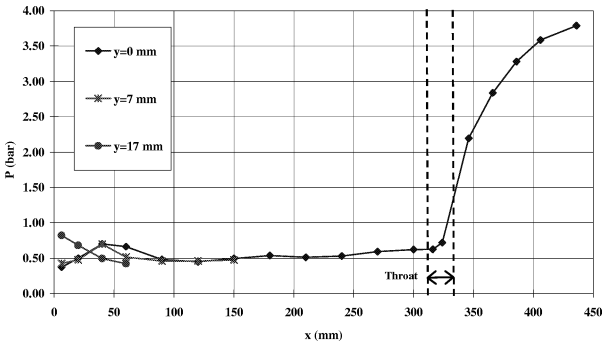

Figure 10. Static pressure profiles in the mixing chamber.

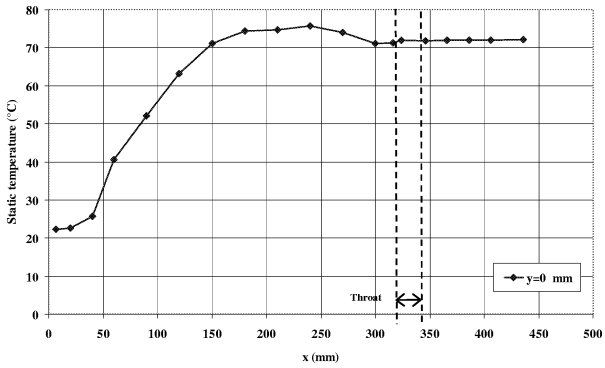

Figure 11. Static temperature profiles in the mixing chamber.

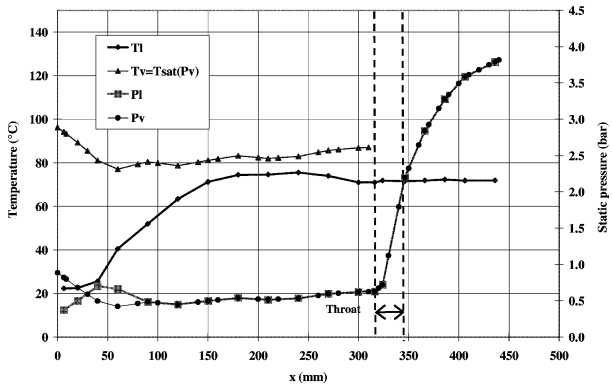

Figure 12. Subcooling between the vapour and liquid phases in the mixing chamber.

drop in specific volume and a pressure decrease which is equal to the increase due to the mixing section convergence. After the throat, *figure 10* shows a high-pressure increase until the final pressure delivered by the steam injector. The downstream pressure has no influence on the flow before the condensation shock until this pressure reached a value for which the mixing flow stops suddenly.

2.4. Static temperature measurement

The static temperature is measured using thermocouples (type K) with an accuracy of ± 1 K. The thermocouple soldering is located at 3 mm from the wall in order to be outside of the thermal boundary layer. Only the liquid temperature on the center line ($y = 0$ mm) is measured because it is impossible to measure accurately the static temperature in the high velocity fields of the vapour or at the interface of the liquid jet (the measurements are always in a range varying from the total temperature to the static temperature). The results for the operating conditions of *table II* are presented in *figure 11*.

The temperature (*figure 11*) of the liquid phase quickly increases at the entrance of the mixing chamber. It proves that the heat transfer between the liquid and vapour phases is very high in the jet atomisation zone. After a complete jet disintegration and when the flow is fully dispersed the temperature does not significantly change.

3. EXPERIMENTAL RESULTS AND PARAMETER CALCULATIONS

The aim of this paragraph is to correlate the set of measured variables in order to understand the physical phenomena occurring in the mixing chamber and to calculate the unknown parameters (mass flow rates and velocities). For this analysis, we have made the following hypotheses:

– the two-phase flow is one-dimensional,

– the liquid temperature is assumed to be equal to the center line measured temperatures $T_{\mathrm{L}} = T_{y=0\ \mathrm{mm}}$,

– the liquid and vapour pressure fields are equal ($P_{\mathrm{V}} = P_{\mathrm{L}}$) in the fully dispersed flow,

– the vapour is saturated: $T_{\mathrm{V}} = T_{\mathrm{sat}}(P_{\mathrm{V}})$.

3.1. Subcooling of the liquid phase

The subcooling is defined as the difference between the saturation temperature at the vapour pressure and the liquid temperature. This subcooling, representative of the thermal non-equilibrium between the phases, is the driving force of the energy and mass transfer (direct condensation).

The subcooling, deduced from the temperature profile (see *figure 12*), may show that the main heat transfer occurs in the zone 0 mm $< x <$ 150 mm. It may be expressed as

$$Q_i = A_i H_{i\mathrm{L}} (T_{\mathrm{V}} - T_{\mathrm{L}}) \qquad (2)$$

with:

- Q_i density of heat flux,
- $H_{i\mathrm{L}}$ heat transfer coefficient,
- A_i interface density area.

Downstream this zone, for $x > 150$ mm, the subcooling becomes nearly constant and equal to 10 K. It shows that the flow is in quasi thermodynamic equilibrium, but this equilibrium is never completely reached.

3.2. Calculation of the mass flow rates and the velocities of the vapour and liquid phases

Two semi-empirical models are developed in order to calculate the mass flow rate and the velocities of both phases:

- a first model based on the conservative variables of the flow,
- a second model based on the heat transfer between the phases.

First model

For a steady flow, the flow is characterised by two invariants, the total mass flow rate M_T and the total energy of the flow $\dot{H}_T$:

$$\begin{cases} M_T = M_V + M_L = C^{ste} \\ \dot{H}_T = M_V\left(h_V + \dfrac{u_V^2}{2}\right) + M_L\left(h_L + \dfrac{u_L^2}{2}\right) = C_{ste} \end{cases} \quad (3)$$

These invariants are calculated from the upstream operating conditions of the injector. Furthermore, we have

$$\begin{cases} M_V = \alpha\rho_V u_V S \\ M_L = (1-\alpha)\rho_L u_L S \end{cases} \quad (4)$$

$$\begin{cases} \rho_V = \rho_{sat}(P_V; x_{V,V}) \\ \rho_L = \rho(P_L; T_L) \cong \rho(T_L) \end{cases} \quad \text{and} \quad \begin{cases} h_V = h_{sat}(P_V; x_{V,V}) \\ h_L = h(P_L; T_L) \cong h(T_L) \end{cases} \quad (5)$$

and writing the intermediate parameters

$$\begin{cases} \varphi_V = \dfrac{1}{\alpha\rho_V S} \\ \varphi_L = \dfrac{1}{(1-\alpha)\rho_L S} \end{cases} \quad (6)$$

the set of equations (3) becomes

$$\begin{cases} M_T = M_V + M_L = C_{ste} \\ \dot{H}_T = M_V\left(h_V + \dfrac{\varphi_V^2 M_V^2}{2}\right) + M_L\left(h_L + \dfrac{\varphi_L^2 M_L^2}{2}\right) \\ \qquad = C_{ste} \end{cases} \quad (7)$$

In this non-linear system, M_V and M_L are unknown and all other variables $(h_V; h_L; \varphi_V; \varphi_L)$ are directly deduced from the measurements, the geometry and the boundary conditions. This system is numerically solved with the Newton–Raphson method. The thermodynamic properties of steam and water are deduced from Schmidt's tables [13]. The last unknowns u_V and u_L are calculated from the knowledge of M_V, M_L and experimental parameters. Thus, all thermohydraulic variables of the flow are determined.

Second model

Condensation of the vapour results in heat transfer to the liquid surface (essentially jet). This model supposes that the temperature increase of the liquid phase is only due to the direct condensation of the vapour, which progressively gives up its latent heat. The vapour mass flow rate variation is also equal to

$$dM_V = S\Gamma_V\,dx = -\frac{M_L C_{PL}(T_L)}{x_{V,V}L(P_V)}\,dT_L \quad (8)$$

with:

- $\Gamma_V = (1/S)(dM_V/dx)$ condensing mass flux of vapour,
- $L(P_V)$ latent heat of vaporisation at P_V,
- C_{PL} liquid specific heat.

The conservation of the total mass flow rate implies the following equation:

$$dM_V = -dM_L \quad (9)$$

By integrating equations (8) and (9) along the mixing chamber (length L_m), we obtain:

$$\begin{cases} M_V = -\displaystyle\int_0^{L_m} \frac{M_L C_{PL}(T_L)}{x_{V,V}L(P_V)}\,dT_L + M_{0V} \\ M_L = -\displaystyle\int_0^{L_m} dM_V + M_{0L} \end{cases} \quad (10)$$

This integral system (10) contains two unknowns $(M_V; M_L)$. Other variables are deduced from the measurements and state equations. As the preceding method, it determines all the thermohydraulic variables in the flow.

Figures 13, *14* and *15* show the mass flow rate for each phase, the velocities and the slip ratio of the two phases, respectively.

In *figure 13* we see that the major part of the vapour phase is condensed in the zone $0 < x < 150$ mm. In *figure 14* we can observe that the vapour is firstly accelerated (effect of the direct condensation), then decelerated when it encounters the liquid phase (momentum

transfer). The liquid phase is always accelerated until the throat. At the abscissa $x = 150$ mm, *figure 15* shows that the slip ratio of the two phases is equal to one, showing that the flow becomes homogeneous after this point. The large velocity fluctuations (see *figure 14*) are due to the sensitivity of temperature measurements in the zone $x > 150$ mm (heat transfer becomes negligible). Consequently, this method is non-adequate for the zone where the flow is in quasi equilibrium.

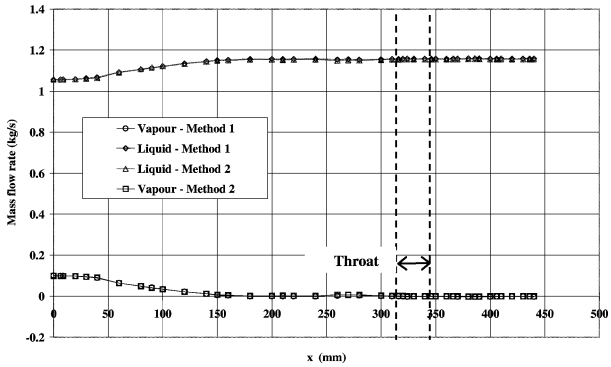

Figure 13. Mass flow rate for each phase (kg·s^{-1}).

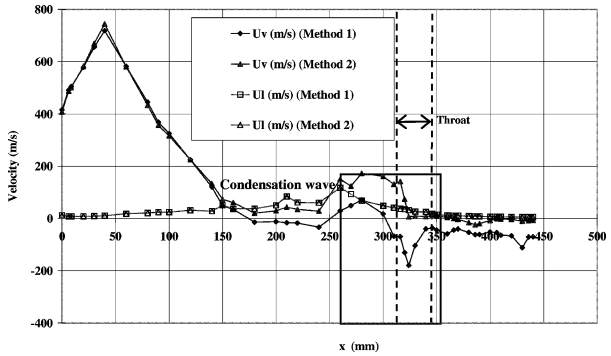

Figure 14. Velocity profiles in the mixing chamber.

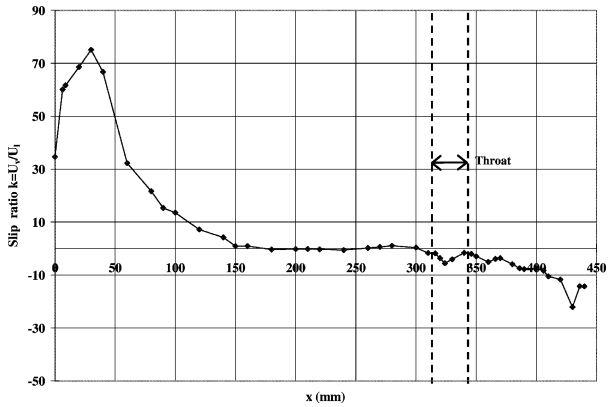

Figure 15. Slip ratio profile in the mixing chamber.

3.3. Non-thermodynamic equilibrium in the dispersed flow and in the condensation wave

The preceding results show that the slip ratio is nearly equal to one when the flow becomes fully dispersed. The flow is also homogeneous. Assuming the hypothesis that the velocities of both phases are equal, the vapour quality can be directly deduced from the void fraction measurements:

$$x_{\mathrm{V}} = \frac{\alpha\rho_{\mathrm{V}}}{\alpha\rho_{\mathrm{V}} + (1-\alpha)\rho_{\mathrm{L}}} \tag{11}$$

The following relations give the mixing velocity and the average density of the mixing flow:

$$u_{\mathrm{m}} = u_{\mathrm{V}} = u_{\mathrm{L}} = \frac{M_{\mathrm{T}}}{\rho_{\mathrm{m}} S} \tag{12}$$

$$\rho_{\mathrm{m}} = \alpha\rho_{\mathrm{V}} + (1-\alpha)\rho_{\mathrm{L}} \tag{13}$$

Quality and velocity profiles for the quasi-equilibrium zone are shown in *figure 16*.

Assuming the hypothesis of a slip ratio equal to one, we obtain coherent results in the quasi equilibrium zone (*figure 16*). The quality profile curve shows that the condensation of the vapour in the mixing flow is achieved after the throat where the condensation wave occurs. This condensation is followed by a strong reduction of the void fraction that increases the density and decelerates the mixing flow. This zone is characterised by a thermodynamic non-equilibrium flow due to a delay of the relaxation time for the condensation. In *figure 17*, we compare

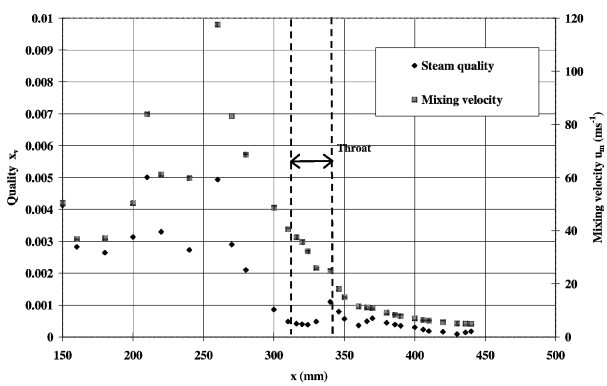

Figure 16. Mixing velocity and vapour quality in the mixing chamber (quasi equilibrium zone).

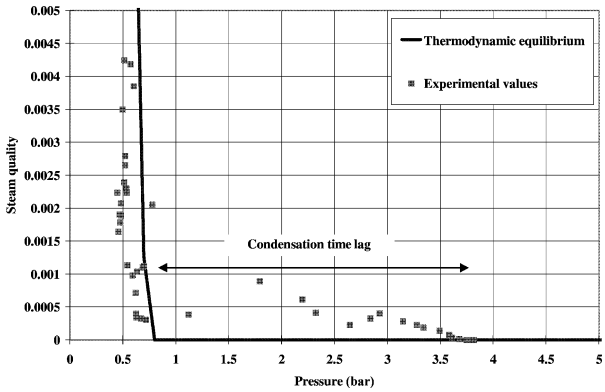

Figure 17. Non-equilibrium flow and condensation time lag in the condensation wave.

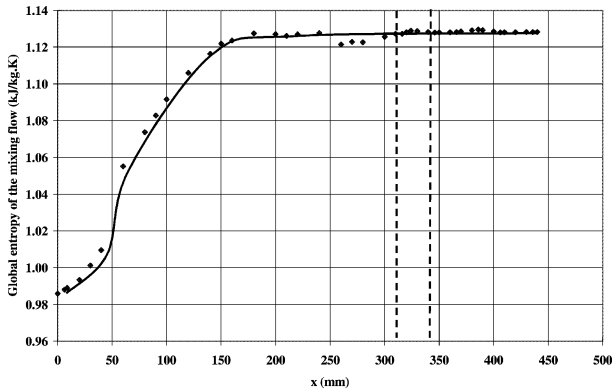

Figure 18. Specific entropy in the mixing chamber.

the real quality x_V and the quality of the flow which is in thermodynamic equilibrium x_v, as a function of the pressure of the flow. The variation of the pressure with the steam quality before the total condensation results in variation of the temperature. We note the presence of (small) vapour mass, which should not be present, if we were at the thermodynamic equilibrium. This phenomenon is responsible of the degradation in the final pressure rise for the steam injector. It implies a compression work for the mixing more important than if the flow was single phase. The final pressure gain is lower than the pressure gain obtained in the absence of condensation relaxation time delay. Our estimation for this time is 5 μs in accordance with the results of Bilicki [14] who previously studied this phenomenon.

3.4. Entropy production of the system in the mixing chamber

From this set of thermohydraulic variables, it is also possible to calculate the entropy production generated by the irreversibilities of the flow in the mixing chamber. The specific entropy of the mixing flow can be calculated as

$$s_m = \frac{M_V s_V + M_L s_L}{(M_V + M_L)} \qquad (14)$$

with:

- $s_V = s(P_V; x_{V,V})$ specific entropy of the vapour phase,
- $s_L = s(P_L; T_L)$ specific entropy of the liquid phase.

The entropy is a very interesting parameter for two reasons:

– analysis of sensitivity shows that this parameter is particularly accurate, because slightly sensitive to measurement variations,

– it permits to verify the coherence of the thermohydraulic variables (measured and calculated) in accordance with the second law.

The evolution of the fluid entropy shown in *figure 18*. On one hand, it shows that the thermohydraulic variables are coherent because the entropy variation is globally increasing. On the other hand, *figure 18* shows that the main entropy production occurs at the entrance of the mixing chamber, where the difference of temperatures (*figure 12)* and velocities (*figure 14*) of both phases are at maximum values. When the flow reaches the quasi-equilibrium zone ($x > 150$ mm), the evolution of the flow can be considered as quasi-isentropic. The condensation wave is finally weakly dissipative, but the pressure in the liquid phase is very sensitive to the entropy variation. For example, for liquid water (pressure 6 bar, temperature 60 °C) an isenthalpic process with an entropy increase of 2 ‰ drives a pressure drop of 5 bar.

4. CONCLUSION

The analysis of the experimental results allows to have a better knowledge of all thermohydraulic variables in the flow and permits to do some simple hypotheses for the modelling of the mixing chamber. The main conclusions of this study are the following:

– at the entrance of the mixing chamber, the flow is characterised by a strong non-equilibrium of temperatures and velocities. This zone is strongly dissipative with high production of irreversibilities;

– quickly, the flow becomes homogeneous and follows a quasi-isentropic evolution. Nevertheless, the thermodynamic equilibrium is never reached by the flow. In particular, we show that a condensation relaxation time is

responsible of the degradation of the pressure recovery in the condensation wave.

This calculation of the thermohydraulic variables will be useful for the source terms of one-dimensional model.

REFERENCES

[1] Deberne N., Léone J.F., Duque A., Lallemand A., A model for calculation of steam injector performance, Int. J. Mult. Phase Flow 25 (1) (1999) 841–855.

[2] Rose R.P., Steam jet pump analysis and experiments, Report WAPD-TM-227, 1960.

[3] Grolmes A., Steam-water condensing-injector performance analysis with supersonic inlet vapor and convergent condensing section, Report ANL-7443, Argonne National Laboratory, 1968.

[4] Alad'yev I.T., Kabakov V.I., Teplov S.V., Investigation of a multijet injector at different ratios of the velocities of the mixing stream and different areas of the mixing chamber exit, Fluid Mech. Soviet Res. 10 (6) (1981) 116–125.

[5] Alad'yev I.T., Kabakov V.I. et al., Investigation of a condensing injector, Fluid Mech. Soviet Res. 10 (6) (1981) 104–115.

[6] Manno V.P., Debhi A.A., A note: A model of steam injector performance, Chem. Engrg. Comm. 95 (1990) 107–119.

[7] Narabayashi T., Ishiyama T., Miyano H., Nei H., Shioiri A., Feasibility and application on steam injector for next-generation reactor, in: 1st JSME/ASME Joint International Conference on Nuclear Engineering, Tokyo, 1991, pp. 23–28.

[8] Chisacof A., Lallemand A., Theoretical aspect for pumping system from ejector, in: Conf. Nat. Termotehnica, Brasov (3) (1997) 71–78.

[9] Léone J.F., Chisacof A., Lallemand A., Pompe à injection de vapeur. Etude expérimentale, in: Congrés Français de Thermique, Paris, 1994, pp. 149–154.

[10] Cattadori G., Galbiati L., Mazzocchi L., Vanini P., A single-stage high pressure steam injector for next generation reactors: Test results and analysis, Int. J. Mult. Phase Flow 21 (4) (1995) 591–606.

[11] Deberne N., Modélisation et expérimentation des injecteurs-condenseurs, Thèse Sci., INSA, Villeurbanne, 2000.

[12] Monote G., Atomisation d'un jet liquide par un jet de gaz coaxial: analyse du mélange, Thèse Sci., Université, Poitiers, 1994.

[13] Schmidt E., Properties of Water and Steam in SI-Units, Springer-Verlag, Berlin, 1969.

[14] Bilicki Z., Kwidzinski R., Mohammadein S.A., Evaluation of the relaxation time of heat and mass exchange in the liquid–vapour bubble flow, Int. J. Heat Mass Tran. 39 (1996) 753–759.